Atmospheric
Chemistry
and Physics
Discussions

1 Widespread air pollutants of the North China Plain during the Asian summer monsoon season:
2   A case study
3
4   Jiarui Wu[1,3], Naifang Bei[2], Xia Li[1,3], Junji Cao[1*], Tian Feng[1], Yichen Wang[1], Xuexi Tie[1], and Guohui Li[1*]
5
6   [1]Key Lab of Aerosol Chemistry and Physics, SKLLQG, Institute of Earth Environment, Chinese Academy of
7   Sciences, Xi'an, China
8   [2]School of Human Settlements and Civil Engineering, Xi'an Jiaotong University, Xi'an, Shaanxi, China
9   [3]University of Chinese Academy of Science, Beijing, China
10
11 [*]Correspondence to: Guohui Li (ligh@ieecas.cn) and Junji Cao (jjcao@ieecas.cn)
12
13
14 **Abstract**: During the Asian summer monsoon season, prevailing southeasterly -
15 southwesterly winds are subject to delivering air pollutants from the North China Plain (NCP)
16 to the Northeast and Northwest China. In the present study, the WRF-CHEM model is used to
17 evaluate contributions of trans-boundary transport of the NCP emissions to the air quality in
18 the Northeast and Northwest China during a persistent air pollution episode from 22 to 28
19 May 2015. The WRF-CHEM model generally performs well in capturing the observed
20 temporal variation and spatial distribution of fine particulate matters ($PM_{2.5}$), ozone (O_3), and
21 NO_2. The simulated temporal variation of aerosol species is also in good agreement with
22 measurements in Beijing during the episode. Model simulations show that the NCP emissions
23 contribute substantially to the $PM_{2.5}$ level in Liaoning and Shanxi provinces, the adjacent
24 downwind areas of the NCP, with an average of 24.2 and 13.9 μg m^{-3} during the episode,
25 respectively. The $PM_{2.5}$ contributions in Jilin and Shaanxi provinces are also appreciable,
26 with an average of 9.6 and 6.5 μg m^{-3}, respectively. The NCP emissions contribute
27 remarkably to the O_3 level in Liaoning province, with an average of 46.5 μg m^{-3}, varying
28 from 23.9 to 69.5 μg m^{-3}. The O_3 level in Shanxi province is also influenced considerably by
29 the NCP emissions, with an average contribution of 35.1 μg m^{-3}. The average O_3
30 contributions of the NCP emissions to Jilin and Shaanxi provinces are 28.7 and 20.7 μg m^{-3},
31 respectively. The effect of the NCP emissions on the air quality in Inner Mongolia is
32 generally insignificant however. Therefore, effective mitigations of the NCP emissions not
33 only improve the local air quality, but also are beneficial to the air quality in the Northeast
34 and Northwest China during the Asian summer monsoon season.
35
36
37
38
39

Atmospheric
Chemistry
and Physics
Discussions

1   Introduction

40

41   With the rapid growth of industrialization, urbanization and transportation, China has

42   experienced severe air pollution with high levels of fine particulate matters ($PM_{2.5}$) and ozone

43   (O_3) recently (e.g., Chan and Yao, 2008; Zhang et al., 2013; Kurokawa et al., 2013; Li et al.,

44   2017b). Although the Chinese State Council has issued the 'Atmospheric Pollution

45   Prevention and Control Action Plan' in September 2013 with the aim of improving China's

46   air quality, heavy haze or photochemical smog still frequently plagues China, especially in

47   the North China Plain (NCP)，Yangtze River Delta (YRD), and Pearl River Delta (PRD).

48   Elevated O_3 and $PM_{2.5}$ concentrations in the atmosphere not only perturb regional and global

49   climates, also exert adverse effects on air quality, ecosystems, and human health (Weinhold,

50   2008; Parrish and Zhu, 2009).

51   The NCP has become one of the most polluted areas in the world due to a large amount

52   of pollutants emissions and frequent occurrence of unfavorable meteorological situations, as

53   well as the topography (e.g., Tang et al., 2012; Zhang et al., 2013; Zhuang et al., 2014; Pu et

54   al., 2015; Long et al., 2016). Heavy haze with extremely high $PM_{2.5}$ concentrations often

55   covers the NCP during wintertime, partially attributable to the coal combustion for domestic

56   heating (e.g., He et al., 2001; Cao et al., 2007; Li et al., 2017a). However, even in summer,

57   with improvement of the evacuation condition and increase of precipitation, photochemical

58   smog with high levels of $PM_{2.5}$ and O_3 still engulfs the NCP (e.g., Gao et al., 2011; Hu et al.,

59   2014; Cao et al., 2015; Wu et al., 2017). The $PM_{2.5}$ concentrations during summertime in the

60   NCP are generally lower than those in winter, but still much higher than 35 μg m^{-3}, the first

61   grade of National Ambient Air Quality Standards (NAAQS) in China (Feng et al., 2016;

62   Wang et al., 2016; Sun et al., 2016). The average summertime $PM_{2.5}$ concentrations in the

63   NCP are 77.0 ± 41.9 in 2013, much more than those in other regions of China and also

64   exceeding the second grade of NAAQS (Hu et al., 2014). In addition, increasing O_3

65   precursors emissions has caused serious O_3 pollution during summertime in the NCP (e.g.,

66   Zhang et al., 2009; Xu et al., 2011; Kurokawa et al., 2013). Li et al. (2017b) have reported

67   that the maximum 1h O_3 concentration exceeds 200 μg m^{-3} in almost all the cities in Eastern

68   China from April to September 2015, mainly concentrated in the NCP and YRD, showing a

69   widespread and persistent O_3 pollution. Ma et al. (2016) have found a growth trend of the

70   surface O_3 at a rural site in the NCP from 2003 to 2015, with an average rate of 1.13 ppb per

71   year. Wu et al., (2017) have shown that the average afternoon O_3 concentration in the summer

72   of 2015 in Beijing is about 163 μg m^{-3}.

73   China is located in a large monsoon domain, and the Asia summer monsoon (ASM) tend

74   to substantially influence the distribution and trans-boundary transport of air pollutants in

75   China. Zhu et al. (2004) have proposed that the summertime high O_3 concentration over

76   Western China is due to the monsoonal transport from Eastern China and long-range

77   transport from South/central Asia and even Europe. Zhao et al. (2010) have also indicated

78   that O_3 transported from South/Central Asia to Western China increases from May to August

79   because of the northward movement of the India summer monsoon. Huang et al. (2015) have

80   suggested that an earlier onset of the ASM would lead to more O_3 enhancement in the lower

81   troposphere over the NCP in later spring and early summer. Numerous studies have also

82   reported that the strength and tempo-spatial extension of the ASM influences the spatial and

83   temporal distribution of aerosol mass concentrations over Eastern China (Cao et al., 2015; Li

84   et al., 2016; Cheng et al., 2016). For example, Zhang et al. (2010) have emphasized that the

85   East ASM plays a major role in determining the seasonal and interannual variations of the

86   $PM_{2.5}$ concentration over Eastern China. Using the GEOS-CHEM model, Zhu et al. (2012)

87   have shown that the weakening of the ASM increases the aerosol concentration in Eastern

88   China. Wu et al. (2016) have pointed out that the regional transport and tempo-spatial

89   distribution of air pollutants are directly influenced by the East Asian monsoon at seasonal,

Atmospheric
Chemistry
and Physics
Discussions

90   inter-annual, and decadal scales.

91   During the ASM season, meteorological conditions are characterized by prevailing

92   southwesterly-southeasterly winds over Eastern China. Air pollutants originated from the

93   NCP are likely to be transported northwards and affect the air quality in its downwind areas,

94   so it is imperative to quantitatively evaluate the effect of the NCP emissions on the air quality

95   in its neighboring regions. Previous studies have concentrated on the composition,

96   characteristics, and sources of the air pollutants over the NCP (e.g., Han et al., 2006; Liu et

97   al., 2012; Zhao et al., 2013; Li et al., 2015). However, few studies have been performed to

98   investigate the effect of trans-boundary transport of air pollutants originated from the NCP on

99   the air quality in the Northeast and Northwest China under the prevailing southerly wind

100   associated with the ASM.

101   In this study, we first analyze the role of synoptic situations during the ASM (from May

102   to September) in the trans-boundary transport over Northern China and further evaluate the

103   contribution of trans-boundary transport of pollutants originated from the NCP to the air

104   quality in the Northeast and Northwest China using the WRF-CHEM model. The model

105   configuration and methodology are described in Section 2. Analysis results and discussions

106   are presented in Section 3, and conclusions are given in Section 4.

107

108   **2   Model and Methodology**

109   **2.1 WRF-CHEM Model and Configuration**

110   A persistent air pollution episode with high levels of $PM_{2.5}$ and O_3 from 22 to 28 May

111   2015 in Northern China is simulated using the WRF-CHEM model which is developed by Li

112   et al. (2010, 2011a, b, 2012) at the Molina Center for Energy and the Environment. Table 1

113   provides detailed model configurations and Figure 1 shows the WRF-CHEM model

114   simulation domain. The further description of the model is presented in Supplementary

Atmospheric
Chemistry
and Physics
Discussions

115   Information (SI).

116   For the discussion convenience, Northern China is divided into 3 regions (Figure S1): 1)

117   the North China Plain (including Beijing, Tianjin, Hebei, Shandong, Henan, the south of

118   Jiangsu and Anhui, hereafter referred to as the NCP), 2) the Northeast China (including

119   Heilongjiang, Jilin, Liaoning and the east part of Inner Mongolia, hereafter referred to as the

120   NEC), and 3) the Northwest China (including Shanxi, Shaanxi and the west part of Inner

121   Mongolia, hereafter referred to as the NWC). During the episode, the observed average daily

122   $PM_{2.5}$ concentration was 75.5 μg m^{-3} and the mean O_3 concentration in the afternoon was

123   151.2 μg m^{-3} in the NCP. Figure S2 presents the distributions of the anthropogenic emission

124   rates of volatile organic compounds (VOCs), nitrogen oxide (NO_x), organic carbon (OC), and

125   SO_2 in Mainland China, showing that the high emission rates of VOCs, NO_x, OC, and SO_2

126   are generally concentrated in the NCP. It is worth noting that uncertainties in the emission

127   inventory used in this study are rather large considering the rapid changes in anthropogenic

128   emissions that are not fully reflected in the current emission inventory and the complexity of

129   pollutants precursors.

130   **2.2 Data and Methodology**

131   In the present study, the model performance is validated using the hourly measurements

132   of O_3, NO_2, and $PM_{2.5}$ concentrations released by the China's Ministry of Environment

133   Protection (China MEP), which can be accessed at http://www.aqistudy.cn/. In addition, the

134   simulated submicron sulfate, nitrate, ammonium, and organic aerosols are compared to the

135   measurements by the Aerodyne Aerosol Chemical Speciation Monitor (ACSM), which was

136   deployed at the National Center for Nanoscience and Technology (NCNST), Chinese

137   Academy of Sciences in Beijing (Figure 1). The observed mass spectra of organic aerosols

138   are analyzed using the Positive Matrix Factorization (PMF) technique and four components

139   are identified: hydrocarbon-like organic aerosol (HOA)，cooking organic aerosol (COA)，coal

140   combustion organic aerosol (CCOA), and oxygenated organic aerosol (OOA). HOA, COA,

141   and CCOA are interpreted as a surrogate of primary organic aerosols (POA), and OOA is a

142   surrogate of secondary organic aerosols (SOA). Furthermore, the reanalysis data from the

143   European Centre for Medium-Range Weather Forecasts (ECMWF) are used to analyze the

144   synoptic patterns during the ASM season from May to September 2015.

145   The mean bias (*MB*), root mean square error (*RMSE*) and the index of agreement (*IOA*)

146   are utilized to evaluate the performance of the WRF-CHEM model simulations against

147   measurements. To assess the contributions of the NCP emissions to the near-surface

148   concentrations of O_3 and $PM_{2.5}$ in the NEC and NWC, the factor separation approach (FSA)

149   is used in this study (Stein and Alpert, 1993; Gabusi et al., 2008; Li et al., 2014a). The

150   detailed description of methodology can be found in SI-2.

151

152   **3   Results and Discussions**

153   **3.1 Synoptic Patterns during the ASM Season**

154   The ASM commences to prevail from May to September each year in China, with strong

155   winds blowing from oceans to Eastern China and bringing warm and moist airflow to the

156   continent. Furthermore, the Western Pacific subtropical high gradually intensifies, and moves

157   from south to north to influence the weather and climate over China, also transporting water

158   vapor from the sea to Eastern China. During the ASM season, due to the influence of the

159   Western Pacific subtropical high, rain belts and associated deep convections move from

160   Southeastern China to Northern China (Ding et al., 1992, 2005; Lau et al., 1988, 1992; Kang

161   et al., 2002). Figure 2 shows the geopotential heights at 500 hPa and mean sea level pressure

162   with wind vectors during the ASM season in 2015. At 500 hPa, the main part of subtropical

163   high, which is represented by the scope of the contour of 5880 geopotential meter, is located

164   in Northwest Pacific Ocean. The mean ridgeline of the Western Pacific subtropical high is

165   located at 25°N, moving from south to north from May to September, which substantially

166   affects the synoptic conditions in China. Flat westerly wind at 500 hPa prevails over the NCP

167   and its surrounding regions, indicating a stable weather condition. The mean sea level

168   pressure shows that most of areas in the NCP are continually influenced by the ASM and the

169   high-pressure system centering in the Western Pacific, causing the prevailing southeasterly -

170   southwesterly wind over the NCP and its surrounding areas. The detailed description of the

171   synoptic conditions during the study episode can be found in SI.

172   In the region controlled by the Western Pacific subtropical high, a subsidence airflow is

173   dominant with calm or weak winds, and the temperature is extremely high due to the strong

174   sunlight, which is favorable for the accumulation and formation of air pollutants. The air

175   pollutants are likely to be transported from south to north under the persistent effect of

176   southerly winds.

177   Figures 3 and 4 present the relationship of $PM_{2.5}$ and O_3 concentrations in the NCP with

178   those in the NEC and NWC during the ASM season from 2013 to 2016, respectively. The

179   observed $PM_{2.5}$ and O_3 concentrations in the NCP exhibit a positive correlation with those in

180   the NEC and NWC, with the correlation coefficients generally exceeding 0.55. There are two

181   possible reasons for the positive correlation of $PM_{2.5}$ and O_3 concentrations between the NCP

182   and its surrounding regions. One is that when the NCP and its neighboring areas are

183   controlled by the same large-scale synoptic pattern, the concentrations of air pollutants

184   generally vary synchronously. The other is the trans-boundary transport of air pollutants

185   originated from the NCP to its surrounding areas due to the southerly wind associated with

186   the ASM. The correlation coefficients of $PM_{2.5}$ and O_3 concentrations in the provinces of the

187   NEC with those in the NCP generally decrease from south to north, with the coefficients of

188   0.69, 0.56 and 0.52 for $PM_{2.5}$, and of 0.86, 0.76, and 0.76 for O_3 in Liaoning, Jilin and

189   Heilongjiang, respectively. The decreasing trend of the correlation coefficients also exists

Atmospheric
Chemistry
and Physics
Discussions

190   from east to west in the NWC, with coefficients of 0.69 and 0.62 for $PM_{2.5}$, and 0.87 and 0.84

191   for O_3 in Shanxi and Shaanxi, respectively. Hence, when severe air pollution occurs in the

192   NCP in summer, the air quality in its adjacent provinces is likely to be deteriorated, possibly

193   caused by the trans-boundary transport of air pollutants originated from the NCP.

194   **3.2 Model performance**

195   **3.2.1 $PM_{2.5}$, O_3 and NO_2 Simulations in Northern China**

196   Figure 5 shows the temporal variations of observed and simulated near-surface $PM_{2.5}$,

197   O_3 and NO_2 concentrations averaged over monitoring sites in Northern China. The

198   WRF-CHEM model generally simulates well the diurnal variation of $PM_{2.5}$ concentrations in

199   Northern China, with *IOA* of 0.90. The model successfully reproduces the temporal variations

200   of surface O_3 concentrations compared with observations in Northern China, e.g., peak O_3

201   concentrations in the afternoon due to active photochemistry and low O_3 concentrations

202   during nighttime caused by the NO_x titration, with *IOA* of 0.98. However, the model

203   underestimation still exists in simulating the O_3 concentration, with a *MB* of -5.3 μg m^{-3}. The

204   model also reasonably yields the NO_2 diurnal profiles, but frequently overestimates the NO_2

205   concentrations in the late evening due to the simulated low PBL height, and underestimates

206   the concentration in the early morning because of the uncertainties in the NO_x emissions. The

207   further analysis of the model performance of $PM_{2.5}$, O_3 and NO_2 concentrations in Northern

208   China can be found in SI.

209   **3.2.2 Aerosol Species Simulations in Beijing**

210   Figure 6 presents the temporal variations of simulated and observed aerosol species at

211   NCNST site in Beijing from 22 to 28 May 2015. Generally, the WRF-CHEM model predicts

212   reasonably the temporal variations of the aerosol species against the measurements,

213   especially for POA and nitrate aerosol, with *IOA*s of 0.81 and 0.90, respectively. The model

214   has difficulties in well simulating the SOA concentrations, with the *IOA* and *MB* of 0.69 and

Atmospheric
Chemistry
and Physics
Discussions

215   -3.6 μg m^{-3}, respectively. It is worth noting that many factors influence the SOA simulation,

216   including measurements, meteorology, precursors emissions, SOA formation mechanisms

217   and treatments (Bei et al., 2012, 2013). The model reasonably tracks the temporal variation of

218   the observed sulfate concentration, but the bias is still large, and the *MB* and *IOA* are -1.2 μg

219   m^{-3} and 0.68, respectively. The sulfate source in the atmosphere is various, including SO_2

220   gas-phase oxidations by hydroxyl radicals (OH) and stabilized criegee intermediates (sCI),

221   aqueous reactions in cloud or fog droplets, and heterogeneous reactions on aerosol surfaces,

222   as well as direct emissions from power plants and industries (Li et al., 2017a). Considering

223   that the model fails to well resolve convective clouds due to the 10-km horizontal resolution,

224   the sulfate formation from the cloud process is generally underestimated. Additionally, large

225   amount of SO_2 is emitted from point sources, such as power plants or agglomerated industrial

226   zones, which is much more sensitive to wind fields simulations (Bei et al., 2010). The model

227   performs reasonably well in simulating the ammonium aerosol, with the *IOA* and *MB* of 0.77

228   and -0.4 μg m^{-3}, respectively.

229   **3.2.3 Simulations of the Spatial Distribution of PM$_{2.5}$ and O$_3$ Concentrations**

230   Figure 7 provides the distributions of calculated and observed near-surface PM$_{2.5}$

231   concentrations along with the simulated wind fields at 08:00 Beijing Time (BJT) from 23 to

232   28 May 2015. The calculated PM$_{2.5}$ spatial patterns generally agree well with the

233   observations at the monitoring sites. The NCP experiences severer PM$_{2.5}$ pollution than its

234   surrounding areas, with PM$_{2.5}$ concentrations frequently exceeding 150 μg m^{-3} in the

235   Beijing-Tianjin-Hebei region. During the study episodes, the pollutants are likely to be

236   transported to the NEC and NWC under the prevailing southwesterly or southeasterly winds

237   in Northern China, causing the PM$_{2.5}$ concentrations in most of areas of the NEC and NWC

238   frequently to be higher than 75 μg m^{-3}.

239   The O_3 concentration during summertime generally reaches its peak from 14:00 to 16:00

240   BJT in Northern China (Figure 5). Figure 8 shows the spatial distribution of calculated and

241   measured near-surface O_3 concentrations at 14:00 BJT from 23 to 28 May 2015, along with

242   the simulated wind fields. Generally, the simulated O_3 spatial patterns are consistent with the

243   observations, but the model overestimation or underestimation still exists. The simulated high

244   O_3 concentrations at 14:00 BJT, exceeding 200 μg m^{-3}, are frequently concentrated in the

245   NCP, which is also consistent with the measurements. The O_3 transport to the NEC and NWC

246   from the NCP is obvious when the winds are southeasterly or southwesterly, inducing the

247   severe O_3 pollution in the NEC and NWC.

248   In general, the simulated variations of $PM_{2.5}$, O_3, NO_2 and aerosol species are in good

249   agreement with observations, indicating that the simulations of meteorological conditions,

250   chemical processes and the emission inventory used in the WRF-CHEM model are

251   reasonable, providing a reliable base for the further investigation.

252   **3.3 Effects of the NCP Emissions on the Air Quality in the NEC and NWC**

253   To evaluate the contribution of the NCP emissions to the air quality in its neighboring

254   areas, four model simulations are performed, including f_{NS} with all anthropogenic

255   emissions from the NCP and non-NCP areas, f_N with anthropogenic emissions from the

256   NCP only, f_S with anthropogenic emissions from the non-NCP areas only, and f_0 without

257   all anthropogenic emissions. Consequently, the air pollutants concentrations in the NEC and

258   NWC can be separated into four components, including contributions from the local

259   emissions (f'_S, $f_S - f_0$), the trans-boundary transport of the NCP emissions (f'_N, $f_N - f_0$),

260   the interactions of these two emissions (f'_{NS}, $f_{NS} - f_N - f_S + f_0$) and the background

261   (f_0).

262   **3.3.1 Contributions of the NCP Emissions to $PM_{2.5}$ Levels in the NEC and NWC**

263   Figure 9 shows the simulated spatial distribution of daily mean $PM_{2.5}$ concentrations

264   contributed by the NCP emissions in the NEC and NWC from 23 to 28 May 2015. The

265   contribution of trans-boundary transport of the NCP emissions to the $PM_{2.5}$ concentration is

266   the most remarkable in Liaoning, frequently exceeding 30 $\mu g\ m^{-3}$ in the most area of the

267   province during the episode. The NCP emissions also considerably influence the $PM_{2.5}$

268   concentration in Jilin, contributing 5~30 $\mu g\ m^{-3}$ in the most area and occasionally exceeding

269   40 $\mu g\ m^{-3}$. The effect of the NCP emissions on the $PM_{2.5}$ level in Shanxi and Shaanxi is

270   increasingly evident from 23 to 28 May 2015, with the contribution of up to 50~60 $\mu g\ m^{-3}$ in

271   southeast of Shanxi and to a lesser extent of 30~40 $\mu g\ m^{-3}$ in the middle part of Shaanxi on

272   27- 28 May. The contribution of trans-boundary transport of the NCP emissions to the $PM_{2.5}$

273   level in Inner Mongolia is not significant, which may be attributed to the location of the low

274   pressure and terrain characteristics. Obviously, the effect of trans-boundary transport shows a

275   stepwise characteristic; the closer to the NCP emission sources, the more remarkable the

276   impact on the downwind areas. As a result, Liaoning and Shanxi provinces are substantially

277   influenced by the NCP emissions, while Jilin and Shaanxi provinces are affected to a lesser

278   extent.

279   The impact of the NCP emissions on the daily average $PM_{2.5}$ concentration in the NEC

280   and NWC is summarized in Table 2. On average, the NCP emissions increase the $PM_{2.5}$

281   concentrations by 24.2, 9.6, 13.9, 6.5, and 2.6 $\mu g\ m^{-3}$ in Liaoning, Jilin, Shanxi, Shaanxi, and

282   Inner Mongolia, respectively. Figure 10 shows the episode-averaged $PM_{2.5}$ percentage

283   contribution from the NCP emissions to the surrounding areas. The NCP emissions markedly

284   affect the air quality in Liaoning, accounting for around 20%-50% of the $PM_{2.5}$ concentration

285   during the episode and with the most substantial impact on the west part of the province. The

286   NCP emissions contribute about 15%-30% of the $PM_{2.5}$ concentration in Jilin. Shanxi

287   province is also remarkably affected by the NCP emissions, with more than 25% of $PM_{2.5}$

288   concentration contributed by the NCP emissions in the most areas. Although Shaanxi

289   province is a little far from the NCP, the NCP emissions still contribute about 10%-35% of

Atmospheric
Chemistry
and Physics
Discussions

290   the PM$_{2.5}$ concentration. The NCP emissions also enhance the PM$_{2.5}$ concentration by 5-50%

291   in the southern edge of Inner Mongolia, which is adjacent to the NCP.

292   **3.3.2 Contributions of the NCP Emissions to O$_3$ Concentrations in the NEC and NWC**

293   Figure 11 shows the simulated spatial distribution of the average afternoon O$_3$

294   concentrations contributed by the NCP emissions from 23 to 28 May 2015. Similar to the

295   PM$_{2.5}$ case, the contribution of the NCP emissions to the O$_3$ formation in Liaoning and Jilin

296   province is increasingly enhanced during the episode (except on 26 May), and on 25 and 27

297   May, the NCP emissions account for more than 70 μg m^{-3} of the O$_3$ concentration in the most

298   areas of Liaoning. On 25 and 28 May, the NCP emissions contribute more than 70 μg m^{-3} of

299   the O$_3$ concentration in some regions of Jilin. A less impact of the NCP emissions on Jilin

300   province on 26 May is due to the weakening of the low pressure. The NCP emissions play a

301   progressively important role in O$_3$ concentrations in Shanxi and Shaanxi provinces during the

302   episode, especially on 27 and 28 May when the contribution can be up to 60 μg m^{-3}. The

303   impact of the NCP emissions on O$_3$ concentrations in Inner Mongolia is insignificant overall.

304   Table 3 summarizes the effects of the NCP emissions on the average afternoon O$_3$

305   concentration in the NEC and NWC from 22 to 28 May 2015. During the episode, the NCP

306   emissions substantially influence the O$_3$ level in Liaoning province, and the afternoon O$_3$

307   contribution is about 46.5 μg m^{-3} on average, ranging from 23.9 to 69.5 μg m^{-3}. The NCP

308   emissions also contribute an average of 28.7 μg m^{-3} to the O$_3$ concentration in Jilin province,

309   varying from 12.4 to 45.7 μg m^{-3}. The contribution of NCP emissions to Shanxi and Shanxi

310   provinces becomes increasingly significant during the episode, with an average of 35.1 μg

311   m^{-3} for Shanxi province and 20.7 μg m^{-3} for Shaanxi province, respectively. The O$_3$

312   concentration in Inner Mongolia is less influenced by the NCP emissions, with an average of

313   8.4 μg m^{-3}. Figure 12 illustrates the episode-averaged afternoon O$_3$ percentage contribution of

314   the NCP emissions to the surrounding areas. In the NEC, the NCP emissions account for

Atmospheric
Chemistry
and Physics
Discussions

315   15-35% of the afternoon O_3 concentration in the most areas of Liaoning province, and 10-30%

316   in Jilin province. In the NWC, the NCP emissions contribute 10-35% of the O_3 concentration

317   in Shanxi province, and 10-25% in Shaanxi. In Inner Mongolia, the impact of the NCP

318   emissions on O_3 formation is small, generally less than 15% except in the southern area

319   adjacent to the NCP and Liaoning province where a contribution of more than 10% is found.

320

321   **4   Summary and Conclusions**

322   Analyses of the synoptic pattern during the ASM season show that the southeasterly –

323   southwesterly winds prevail in Northern China, facilitating the trans-boundary transport of air

324   pollutants from the NCP to the NEC and NWC. The good relationships of $PM_{2.5}$ and O_3

325   concentrations in the NCP with those in the NEC and NWC during the ASM season also

326   indicate the possibility that the air quality in the NEC and NWC is influenced by the

327   trans-boundary transport of air pollutants originated from the NCP.

328   A widespread and severe pollution episode from 22 to 28 May 2015 in Northern China

329   is further simulated using the WRF-CHEM model to investigate the impact of trans-boundary

330   transport of the NCP emissions on $PM_{2.5}$ and O_3 concentrations in the NEC and NWC, when

331   the region is affected by prevailing southeasterly-southwesterly winds associated with the

332   ASM.

333   In general, the WRF-CHEM model well reproduces the temporal variations and spatial

334   distributions of $PM_{2.5}$, O_3, and NO_2 concentrations compared to observations in Northern

335   China, although the model biases still exist due to the uncertainties in simulated

336   meteorological fields and the emission inventory. The model also performs reasonably well in

337   simulating the variations of aerosol constituents against the ACSM measurement at the

338   NCNST site in Beijing.

Atmospheric
Chemistry
and Physics
Discussions

339   The FSA method is used to investigate the contribution of trans-boundary transport of

340   the NCP emissions to O_3 and $PM_{2.5}$ levels in the NEC and NWC. Model results show that the

341   NCP emissions contribute approximately an average of 24.2 and 13.9 μg m^{-3} to the $PM_{2.5}$

342   concentration in Liaoning and Shanxi during the episode, respectively. The NCP emissions

343   enhance the $PM_{2.5}$ level by 9.6 and 6.5 μg m^{-3} in Jilin and Shaanxi on average, respectively.

344   The NCP emissions also substantially influence the O_3 concentration in the NEC and NWC.

345   The NCP emissions increase the afternoon (12:00 - 18:00 BJT) O_3 concentration in Liaoning

346   by 46.5 μg m^{-3} on average during the episode, followed by 35.1 μg m^{-3} in Shanxi, 28.7 μg m^{-3}

347   in Jilin, and 20.7 μg m^{-3} in Shaanxi. In contrast, the contribution of trans-boundary transport

348   of the NCP emissions to the $PM_{2.5}$ and O_3 concentration in Inner Mongolia are less, with an

349   average of 2.6 and 8.4 μg m^{-3}, respectively. Our results demonstrate that when southerly

350   winds are prevailing in Northern China, air pollutants originated from the NCP are likely to

351   be transported northwards and profoundly affect the air quality in the NEC and NWC.

352   Stringent control of the NCP emissions not only mitigates the local air pollution, also is

353   beneficial to the air quality in the NEC and NWC during the ASM season.

354   Although the model performs well in simulating $PM_{2.5}$, O_3 and NO_2 during the episode

355   in northern China, the uncertainties from meteorological fields and the emission inventory

356   still exist. Future studies need to be conducted to improve the WRF-CHEM model

357   simulations, and to further assess the contributions of trans-boundary transport of the NCP

358   emissions under specific synoptic patterns, considering the rapid changes in anthropogenic

359   emissions, which is not reflected in the present study. Therefore, more episode simulations

360   during the ASM season should be performed to comprehensively evaluate the contribution of

361   trans-boundary transport of the NCP emissions to the air quality in its downwind regions and

362   support the design and implementation of effective emission control strategies.

363

Atmospheric
Chemistry
and Physics
Discussions

371
372
373
374
375

Atmospheric
Chemistry
and Physics
Discussions

376 **Reference**

377 Bei, N., Lei, W., Zavala, M., and Molina, L. T.: Ozone predictabilities due to meteorological
378   uncertainties in the Mexico City basin using ensemble forecasts, Atmospheric Chemistry
379   and Physics, 10, 6295-6309, 10.5194/acp-10-6295-2010, 2010.

380 Bei, N., Li, G., and Molina, L. T.: Uncertainties in SOA simulations due to meteorological
381   uncertainties in Mexico City during MILAGRO-2006 field campaign, Atmospheric
382   Chemistry and Physics, 12, 11295-11308, 10.5194/acp-12-11295-2012, 2012.

383 Bei, N. F., Li, G. H., Zavala, M., Barrera, H., Torres, R., Grutter, M., Gutierrez, W., Garcia,
384   M., Ruiz-Suarez, L. G., Ortinez, A., Guitierrez, Y., Alvarado, C., Flores, I., and Molina, L.
385   T.: Meteorological overview and plume transport patterns during Cal-Mex 2010,
386   Atmospheric Environment, 70, 477-489, 10.1016/j.atmosenv.2012.01.065, 2013.

387 Cao, Z. Q., Sheng, L. F., Liu, Q., Yao, X. H., and Wang, W. C.: Interannual increase of
388   regional haze-fog in North China Plain in summer by intensified easterly winds and
389   orographic forcing, Atmospheric Environment, 122, 154-162,
390   10.1016/j.atmosenv.2015.09.042, 2015.

391 Cao, J. J., Lee, S. C., Chow, J. C., Watson, J. G., Ho, K. F., Zhang, R. J., Jin, Z. D., Shen, Z.
392   X., Chen, G. C., and Kang, Y. M.: Spatial and seasonal distributions of carbonaceous
393   aerosols over China, Journal of Geophysical Research Atmospheres, 112, 22-11, 2007.

394 Chan, C. K., and Yao, X.: Air pollution in mega cities in China, Atmospheric Environment,
395   42, 1-42, 2008.

396 Chen, F., and Dudhia, J.: Coupling an advanced land surface-hydrology model with the Penn
397   State-NCAR MM5 modeling system. Part I: Model implementation and sensitivity,
398   Monthly Weather Review, 129, 569-585,
399   10.1175/1520-0493(2001)129<0569:caalsh>2.0.co;2, 2001.

400 Cheng, X. G., Zhao, T. L., Gong, S. L., Xu, X. D., Han, Y. X., Yin, Y., Tang, L. L., He, H. C.,
401   and He, J. H.: Implications of East Asian summer and winter monsoons for interannual
402   aerosol variations over central-eastern China, Atmospheric Environment, 129, 218-228,
403   10.1016/j.atmosenv.2016.01.037, 2016.

404 Chou, M. D., and Suarez, M. J.: A solar radiation parameterization for atmospheric studies,
405   NASA TM-104606, Nasa Tech.memo, 15, 1999.

406 Chou, M. D., Suarez, M. J., Liang, X. Z., Yan, M. H., and Cote, C.: A Thermal Infrared
407   Radiation Parameterization for Atmospheric Studies, Max J, 2001.

408 Ding, Y. H.: Summer monsoon rainfalls in china, Journal of Meteorological Society of Japan,
409   70, 373-396, 1992.

410 Ding, Y. H., and Chan, J. C. L.: The East Asian summer monsoon: an overview, Meteorology
411   and Atmospheric Physics, 89, 117-142, 10.1007/s00703-005-0125-z, 2005.

412 Feng, T., Bei, N. F., Huang, R. J., Cao, J. J., Zhang, Q., Zhou, W. J., Tie, X. X., Liu, S. X.,
413   Zhang, T., Su, X. L., Lei, W. F., Molina, L. T., and Li, G. H.: Summertime ozone
414   formation in Xi'an and surrounding areas, China, Atmospheric Chemistry and Physics, 16,
415   4323-4342, 10.5194/acp-16-4323-2016, 2016.

416 Gabusi, V., Pisoni, E., and Volta, M.: Factor separation in air quality simulations, Ecological
417   Modelling, 218, 383-392, 10.1016/j.ecolmodel.2008.07.030, 2008.

Atmospheric
Chemistry
and Physics
Discussions

418 Gao, Y., Liu, X., Zhao, C., and Zhang, M.: Emission controls versus meteorological
419   conditions in determining aerosol concentrations in Beijing during the 2008 Olympic
420   Games, Atmospheric Chemistry and Physics, 11, 12437-12451,
421   10.5194/acp-11-12437-2011, 2011.

422 Guenther, A., Karl, T., Harley, P., Wiedinmyer, C., Palmer, P. I., and Geron, C.: Estimates of
423   global terrestrial isoprene emissions using MEGAN (Model of Emissions of Gases and
424   Aerosols from Nature), Atmospheric Chemistry and Physics, 6, 3181-3210, 2006.

425 Han, J. S., Moon, K. J., Lee, S. J., Kim, Y. J., Ryu, S. Y., Cliff, S. S., and Yi, S. M.:
426   Size-resolved source apportionment of ambient particles by positive matrix factorization
427   at Gosan background site in East Asia, Atmospheric Chemistry and Physics, 6, 211-223,
428   2006.

429 He, K., Yang, F., Ma, Y., Zhang, Q., Yao, X., Chan, C. K., Cadle, S., Chan, T., and Mulawa,
430   P.: The characteristics of PM2.5 in Beijing, China, Atmospheric Environment, 35,
431   4959-4970, 2001.

432 Hong, S.-Y., and Lim, J.-O. J.: The WRF Single-Moment 6-Class Microphysics Scheme
433   (WSM6), Asia-Pacific Journal of Atmospheric Sciences, 42, 129-151, 2006.

434 Horowitz, L. W., Walters, S., Mauzerall, D. L., Emmons, L. K., Rasch, P. J., Granier, C., Tie,
435   X. X., Lamarque, J. F., Schultz, M. G., Tyndall, G. S., Orlando, J. J., and Brasseur, G. P.:
436   A global simulation of tropospheric ozone and related tracers: Description and evaluation
437   of MOZART, version 2, Journal of Geophysical Research-Atmospheres, 108, 29,
438   10.1029/2002jd002853, 2003.

439 Hu, J. L., Wang, Y. G., Ying, Q., and Zhang, H. L.: Spatial and temporal variability of PM2.5
440   and PM10 over the North China Plain and the Yangtze River Delta, China, Atmospheric
441   Environment, 95, 598-609, 10.1016/j.atmosenv.2014.07.019, 2014.

442 Huang, J., Liu, H., Crawford, J. H., Chan, C., Considine, D. B., Zhang, Y., Zheng, X., Zhao,
443   C., Thouret, V., Oltmans, S. J., Liu, S. C., Jones, D. B. A., Steenrod, S. D., and Damon,
444   M. R.: Origin of springtime ozone enhancements in the lower troposphere over Beijing:
445   in situ measurements and model analysis, Atmospheric Chemistry and Physics, 15,
446   5161-5179, 10.5194/acp-15-5161-2015, 2015.

447 Janjić, Z. I.: Nonsingular Implementation of the Mellor–Yamada Level 2.5 Scheme in the
448   NCEP Meso Model, Ncep Office Note, 436, 2002.

449 Kang, I. S., Jin, K., Wang, B., Lau, K. M., Shukla, J., Krishnamurthy, V., Schubert, S. D.,
450   Wailser, D. E., Stern, W. F., Kitoh, A., Meehl, G. A., Kanamitsu, M., Galin, V. Y.,
451   Satyan, V., Park, C. K., and Liu, Y.: Intercomparison of the climatological variations of
452   Asian summer monsoon precipitation simulated by 10 GCMs, Climate Dynamics, 19,
453   383-395, 10.1007/s00382-002-0245-9, 2002.

454 Kurokawa, J., Ohara, T., Morikawa, T., Hanayama, S., Janssens-Maenhout, G., Fukui, T.,
455   Kawashima, K., and Akimoto, H.: Emissions of air pollutants and greenhouse gases over
456   Asian regions during 2000-2008: Regional Emission inventory in ASia (REAS) version 2,
457   Atmospheric Chemistry and Physics, 13, 11019-11058, 10.5194/acp-13-11019-2013,
458   2013.

459 Lau, K. M., Yang, G. J., and Shen, S. H.: Seasonal and intraseasonal climatology of summer
460   monsoon rainfall over East-Asia, Monthly Weather Review, 116, 18-37,
461   10.1175/1520-0493(1988)116<0018:saicos>2.0.co;2, 1988.

462 Lau, K. M.: East-asian summer monsoon rainfall variability and climate teleconnection,
463   Journal of Meteorological Society of Japan, 70, 211-242, 1992.

464 Li, G., Lei, W., Zavala, M., Volkamer, R., Dusanter, S., Stevens, P., and Molina, L. T.:
465   Impacts of HONO sources on the photochemistry in Mexico City during the
466   MCMA-2006/MILAGO Campaign, Atmospheric Chemistry and Physics, 10, 6551-6567,
467   10.5194/acp-10-6551-2010, 2010.

468 Li, G., Bei, N., Tie, X., and Molina, L. T.: Aerosol effects on the photochemistry in Mexico
469   City during MCMA-2006/MILAGRO campaign, Atmospheric Chemistry and Physics, 11,
470   5169-5182, 10.5194/acp-11-5169-2011, 2011a.

471 Li, G., Zavala, M., Lei, W., Tsimpidi, A. P., Karydis, V. A., Pandis, S. N., agaratna, M. R.,
472   and Molina, L. T.: Simulations of organic aerosol concentrations in Mexico City using
473   the WRF-CHEM model during the MCMA-2006/MILAGRO campaign, Atmospheric
474   Chemistry and Physics, 11, 3789-3809, 10.5194/acp-11-3789-2011, 2011b.

475 Li, G., Lei, W., Bei, N., and Molina, L. T.: Contribution of garbage burning to chloride and
476   PM2.5 in Mexico City, Atmospheric Chemistry and Physics, 12, 8751-8761,
477   10.5194/acp-12-8751-2012, 2012.

478 Li, G. H., Bei, N. F., Zavala, M., and Molina, L. T.: Ozone formation along the California
479   Mexican border region during Cal-Mex 2010 field campaign, Atmospheric Environment,
480   88, 370-389, 10.1016/j.atmosenv.2013.11.067, 2014.

481 Li, G., Bei, N., Cao, J., Huang, R., Wu, J., Feng, T., Wang, Y., Liu, S., Zhang, Q., and Tie, X.:
482   A possible pathway for rapid growth of sulfate during haze days in China, Atmospheric
483   Chemistry & Physics, 17, 1-43, 2017a.

484 Li, G., Bei, N., Cao, J., Wu, J., Long, X., Feng, T., Dai, W., Liu, S., Zhang, Q., and Tie, X.:
485   Widespread and persistent ozone pollution in eastern China during the non-winter season
486   of 2015: observations and source attributions, Atmospheric Chemistry & Physics, 17,
487   1-39, 2017b.

488 Li, J., Xie, S. D., Zeng, L. M., Li, L. Y., Li, Y. Q., and Wu, R. R.: Characterization of
489   ambient volatile organic compounds and their sources in Beijing, before, during, and after
490   Asia-Pacific Economic Cooperation China 2014, Atmospheric Chemistry and Physics, 15,
491   7945-7959, 10.5194/acp-15-7945-2015, 2015.

492 Li, H., Zhang, Q., Zhang, Q., Chen, C., Wang, L., Wei, Z., Zhou, S., Parworth, C., Zheng, B.,
493   and Canonaco, F.: Wintertime aerosol chemistry and haze evolution in an extremely
494   polluted city of the North China Plain: significant contribution from coal and biomass
495   combustion, Atmospheric Chemistry and Physics, 17, 1-31, 2017a.

496 Li, Z. Q., Lau, W. K. M., Ramanathan, V., Wu, G., Ding, Y., Manoj, M. G., Liu, J., Qian, Y.,
497   Li, J., Zhou, T., Fan, J., Rosenfeld, D., Ming, Y., Wang, Y., Huang, J., Wang, B., Xu, X.,
498   Lee, S. S., Cribb, M., Zhang, F., Yang, X., Zhao, C., Takemura, T., Wang, K., Xia, X.,
499   Yin, Y., Zhang, H., Guo, J., Zhai, P. M., Sugimoto, N., Babu, S. S., and Brasseur, G. P.:
500   Aerosol and monsoon climate interactions over Asia, Reviews of Geophysics, 54,
501   866-929, 10.1002/2015rg000500, 2016.

502 Liu, Z., Wang, Y., Gu, D., Zhao, C., Huey, L. G., Stickel, R., Liao, J., Shao, M., Zhu, T.,
503   Zeng, L., Amoroso, A., Costabile, F., Chang, C. C., and Liu, S. C.: Summertime
504   photochemistry during CAREBeijing-2007: ROx budgets and O_3 formation, Atmospheric
505   Chemistry and Physics, 12, 7737-7752, 10.5194/acp-12-7737-2012, 2012.

Long, X., Tie, X. X., Cao, J. J., Huang, R. J., Feng, T., Li, N., Zhao, S. Y., Tian, J., Li, G. H., and Zhang, Q.: Impact of crop field burning and mountains on heavy haze in the North China Plain: a case study, Atmospheric Chemistry and Physics, 16, 9675-9691, 10.5194/acp-16-9675-2016, 2016.

Ma, Z., Xu, J., Quan, W., Zhang, Z., Lin, W., and Xu, X.: Significant increase of surface ozone at a rural site, north of eastern China, Atmospheric Chemistry and Physics, 16, 3969-3977, 2016.

Parrish, D. D., and Zhu, T.: Clean Air for Megacities, Science, 326, 674-675, 10.1126/science.1176064, 2009.

Pu, W. W., Zhao, X. J., Shi, X. F., Ma, Z. Q., Zhang, X. L., and Yu, B.: Impact of long-range transport on aerosol properties at a regional background station in Northern China, Atmospheric Research, 153, 489-499, 10.1016/j.atmosres.2014.10.010, 2015.

Stein, U., and Alpert, P.: Factor separation in numerical simulations, Journal of the Atmospheric Science, 50, 2107-2115, 10.1175/1520-0469(1993) 050<2107:fsins>2.0.co;2, 1993.

Sun, Y., Jiang, Q., Xu, Y., Ma, Y., Zhang, Y., Liu, X., Li, W., Wang, F., Li, J., and Wang, P.: Aerosol characterization over the North China Plain: Haze life cycle and biomass burning impacts in summer, Journal of Geophysical Research Atmospheres, 121, n/a-n/a, 2016.

Tang, G., Wang, Y., Li, X., Ji, D., Hsu, S., and Gao, X.: Spatial-temporal variations in surface ozone in Northern China as observed during 2009-2010 and possible implications for future air quality control strategies, Atmospheric Chemistry and Physics, 12, 2757-2776, 10.5194/acp-12-2757-2012, 2012.

Wang, Z. S., Zhang, D. W., Li, Y. T., Dong, X., Sun, R. W., and Sun, N. D.: Different air pollution situations of O_3 and $PM_{2.5}$ during summer in Beijing, 2016.

Weinhold, B.: Ozone nation - EPA standard panned by the people, Environmental Health Perspectives, 116, A302-A305, 2008.

Wu, G. X., Li, Z. Q., Fu, C. B., Zhang, X. Y., Zhang, R. Y., Zhang, R. H., Zhou, T. J., Li, J. P., Li, J. D., Zhou, D. G., Wu, L., Zhou, L. T., He, B., and Huang, R. H.: Advances in studying interactions between aerosols and monsoon in China, Science China-Earth Sciences, 59, 1-16, 10.1007/s11430-015-5198-z, 2016.

Wu, J., Li, G., Cao, J., Bei, N., Wang, Y., Feng, T., Huang, R., Liu, S., Zhang, Q., and Tie, X.: Contributions of trans-boundary transport to summertime air quality in Beijing, China, Atmospheric Chemistry and Physics, 17, 1-46, 2017.

Xu, J., Zhang, X. L., Xu, X. F., Zhao, X. J., Meng, W., and Pu, W. W.: Measurement of surface ozone and its precursors in urban and rural sites in Beijing, in: Second International Conference on Mining Engineering and Metallurgical Technology, edited by: Zhu, R., Procedia Earth and Plantetary Science, Elsevier Science Bv, Amsterdam, 255-261, 2011.

Zhang, L., Liao, H., and Li, J. P.: Impacts of Asian summer monsoon on seasonal and interannual variations of aerosols over eastern China, Journal of Geophysical Research-Atmospheres, 115, 20, 10.1029/2009jd012299, 2010.

Zhang, Q., Streets, D. G., Carmichael, G. R., He, K. B., Huo, H., Kannari, A., Klimont, Z., Park, I. S., Reddy, S., Fu, J. S., Chen, D., Duan, L., Lei, Y., Wang, L. T., and Yao, Z. L.:

Atmospheric
Chemistry
and Physics
Discussions

Open Access

549   Asian emissions in 2006 for the NASA INTEX-B mission, Atmospheric Chemistry and
550   Physics, 9, 5131-5153, 2009.

551   Zhang, R., Jing, J., Tao, J., Hsu, S. C., Wang, G., Cao, J., Lee, C. S. L., Zhu, L., Chen, Z.,
552   Zhao, Y., and Shen, Z.: Chemical characterization and source apportionment of PM2.5 in
553   Beijing: seasonal perspective, Atmospheric Chemistry and Physics, 13, 7053-7074,
554   10.5194/acp-13-7053-2013, 2013.

555   Zhao, C., Wang, Y. H., Yang, Q., Fu, R., Cunnold, D., and Choi, Y.: Impact of East Asian
556   summer monsoon on the air quality over China: View from space, Journal of Geophysical
557   Research-Atmospheres, 115, 12, 10.1029/2009jd012745, 2010.

558   Zhao, X. J., Zhao, P. S., Xu, J., Meng, W., Pu, W. W., Dong, F., He, D., and Shi, Q. F.:
559   Analysis of a winter regional haze event and its formation mechanism in the North China
560   Plain, Atmospheric Chemistry and Physics, 13, 5685-5696, 10.5194/acp-13-5685-2013,
561   2013.

562   Zhu, B., Akimoto, H., Wang, Z., Sudo, K., Tang, J., and Uno, I.: Why does surface ozone
563   peak in summertime at Waliguan?, Geophysical Research Letters, 31, 4,
564   10.1029/2004gl020609, 2004.

565   Zhu, J. L., Liao, H., and Li, J. P.: Increases in aerosol concentrations over eastern China due
566   to the decadal-scale weakening of the East Asian summer monsoon, Geophysical
567   Research Letters, 39, 6, 10.1029/2012gl051428, 2012.

568   Zhuang, X. L., Wang, Y. S., He, H., Liu, J. G., Wang, X. M., Zhu, T. Y., Ge, M. F., Zhou, J.,
569   Tang, G. Q., and Ma, J. Z.: Haze insights and mitigation in China: An overview, Journal
570   of Environmental Sciences, 26, 2-12, 10.1016/s1001-0742(13)60376-9, 2014.

571

Atmospheric
Chemistry
and Physics
Discussions

Open Access

572

573   Table 1 WRF-CHEM model configurations

574

Regions	Northern China
Simulation period	May 22 to 28, 2015
Domain size	350 × 350
Domain center	35°N, 114°E
Horizontal resolution	10km × 10km
Vertical resolution	35 vertical levels with a stretched vertical grid with spacing ranging from 30 m near the surface, to 500 m at 2.5 km and 1 km above 14 km
Microphysics scheme	WSM 6-class graupel scheme (Hong and Lim, 2006)
Boundary layer scheme	MYJ TKE scheme (Janjić, 2002)
Surface layer scheme	MYJ surface scheme (Janjić, 2002)
Land-surface scheme	Unified Noah land-surface model (Chen and Dudhia, 2001)
Longwave radiation scheme	Goddard longwave scheme (Chou and Suarez, 2001)
Shortwave radiation scheme	Goddard shortwave scheme (Chou and Suarez, 1999)
Meteorological boundary and initial conditions	NCEP 1°×1° reanalysis data
Chemical initial and boundary conditions	MOZART 6-hour output (Horowitz et al., 2003)
Anthropogenic emission inventory	SAPRC-99 chemical mechanism emissions (Zhang et al., 2009)
Biogenic emission inventory	MEGAN model developed by Guenther et al. (2006)
Model spin-up time	28 hours

575

576

577

578 Table 2 Daily average $PM_{2.5}$ contributions ($\mu g\ m^{-3}$) in the NEC and NWC from the NCP
579 emissions from 22 to 28 May 2015.
580

Date	Jilin	Liaoning	Shanxi	Shaanxi	Inner Mongolia
22	0.7	6.1	0.7	0.1	0.2
23	6.1	15.4	4.7	0.5	1.0
24	10.0	19.6	12.7	3.5	2.2
25	14.4	33.6	14.6	6.0	2.6
26	6.4	24.1	16.3	9.1	1.9
27	11.4	46.7	20.7	11.6	3.2
28	18.0	23.7	27.5	14.9	6.9
Average	9.6	24.2	13.9	6.5	2.6

581

582

583

584

Atmospheric
Chemistry
and Physics
Discussions

585 Table 3 Daily afternoon (12:00-18:00 BJT) average O_3 contributions ($\mu g\ m^{-3}$) in the NEC and
586 NWC from the NCP emissions from 22 to 28 May 2015.
587

Date	Jilin	Liaoning	Shanxi	Shaanxi	Inner Mongolia
22	12.4	23.9	12.7	7.7	2.8
23	25.8	38.9	21.5	13.1	5.1
24	35.0	47.5	31.3	21.2	8.5
25	45.7	69.5	39.7	21.5	9.9
26	16.6	41.0	36.4	21.7	10.8
27	23.9	69.3	51.7	33.5	9.6
28	41.7	35.1	52.3	26.5	12.2
Average	28.7	46.5	35.1	20.7	8.4

588
589

Atmospheric
Chemistry
and Physics
Discussions

Figure Captions

590

591   Figure 1 WRF-CHEM simulation domain with topography. The blue circles represent centers
592   of cities with ambient monitoring sites and the red circle denotes the NCNST site. The
593   size of the blue circle represents the number of ambient monitoring sites of cities.

594   Figure 2 (a) Geopotential heights and (b) the mean sea level pressures with wind vectors
595   during the summer monsoon season in 2015.

596   Figure 3 Relationships of observed $PM_{2.5}$ and O_3 concentrations in NCP with those in the
597   NEC during May to September from 2013 to 2016.

598   Figure 4 Same as Figure 3, but for the NWC.

599   Figure 5 Comparison of measured (black dots) and predicted (blue line) diurnal profiles of
600   near-surface hourly (a) $PM_{2.5}$, (b) O_3, and (c) NO_2 averaged over all ambient
601   monitoring stations in Northern China from 22 to 28 May 2015.

602   Figure 6 Comparison of measured (black dots) and simulated (black line) diurnal profiles of
603   submicron aerosol species of (a) POA, (b) SOA, (c) sulfate, (d) nitrate, and (e)
604   ammonium at NCNST site in Beijing from 22 to 28 May 2015.

605   Figure 7 Pattern comparison of simulated vs. observed near-surface $PM_{2.5}$ at 08:00 BJT
606   during from 23 to 28 May 2015. Colored circles: $PM_{2.5}$ observations; color contour:
607         $PM_{2.5}$ simulations; black arrows: simulated surface winds.

608   Figure 8 Same as Figure 7, but for the near-surface O_3 at 14:00 BJT.

609   Figure 9 Contributions of NCP emissions to the daily mean near-surface $PM_{2.5}$ concentration
610   in the NEC and NWC from 23 to 28 May 2015.

611   Figure 10 Average percentage contribution of NCP emissions to $PM_{2.5}$ concentrations in the
612   NEC and NWC fron 22 to 28 May 2015.

613   Figure 11 Same as Figure 9, but for the afternoon (12-18:00 BJT) O_3 concentration.

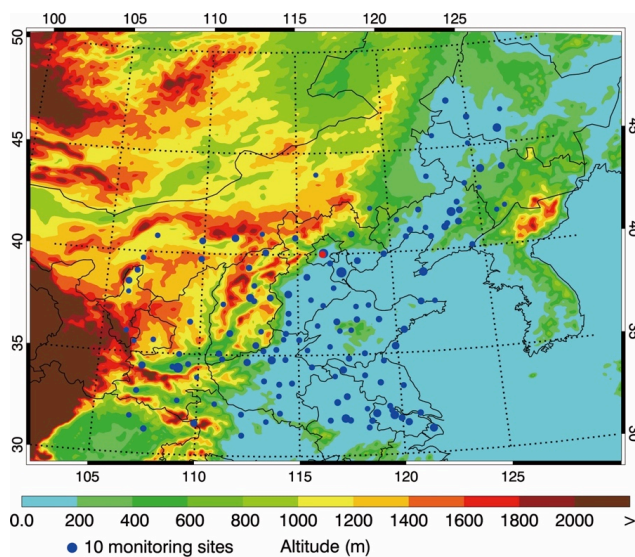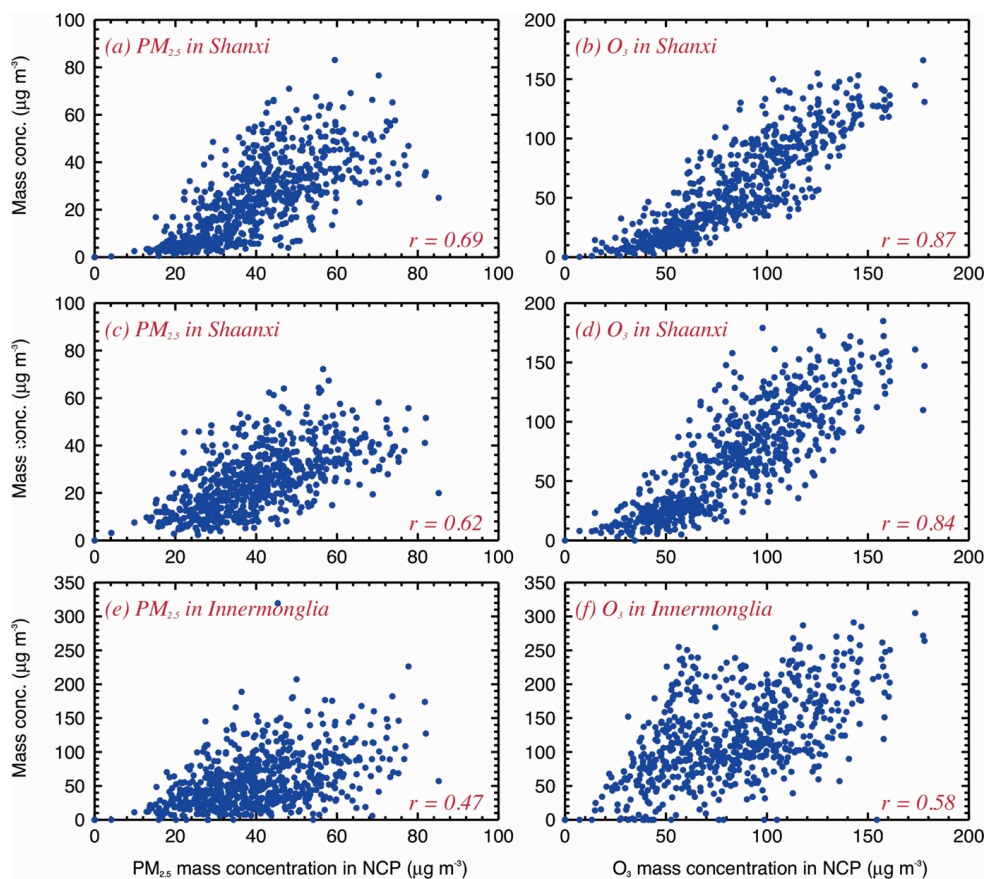614   Figure 12 Same as Figure 10, but for the afternoon (12-18:00 BJT) O_3 concentration.

615
616
617
618
619

Atmospheric
Chemistry
and Physics
Discussions

Open Access

620

621

622 Figure 1 WRF-CHEM simulation domain with topography. The blue circles represent centers
623 of cities with ambient monitoring sites and the red circle denotes the NCNST site. The size of
624 the blue circle represents the number of ambient monitoring sites of cities.

625

626

627

628

629

Atmospheric
Chemistry
and Physics

Discussions
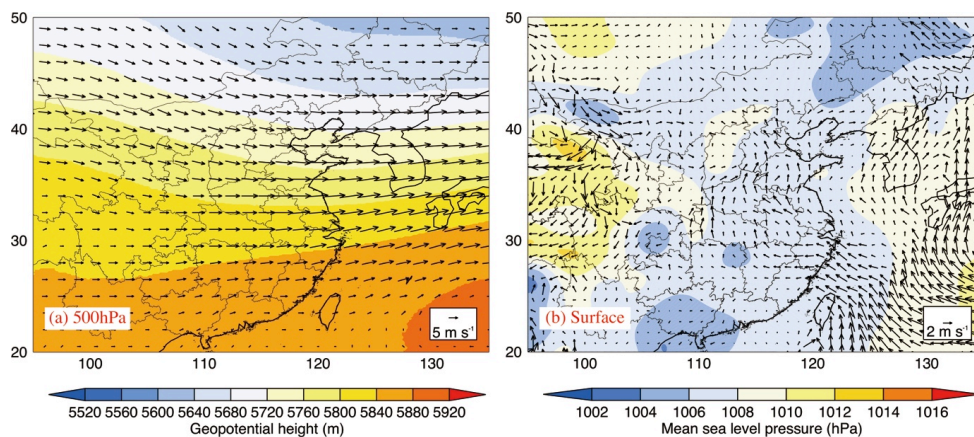
630

631

632 Figure 2 (a) Geopotential heights and (b) the mean sea level pressures with wind vectors
633 during the summer monsoon season in 2015.

634

635

636

637

638
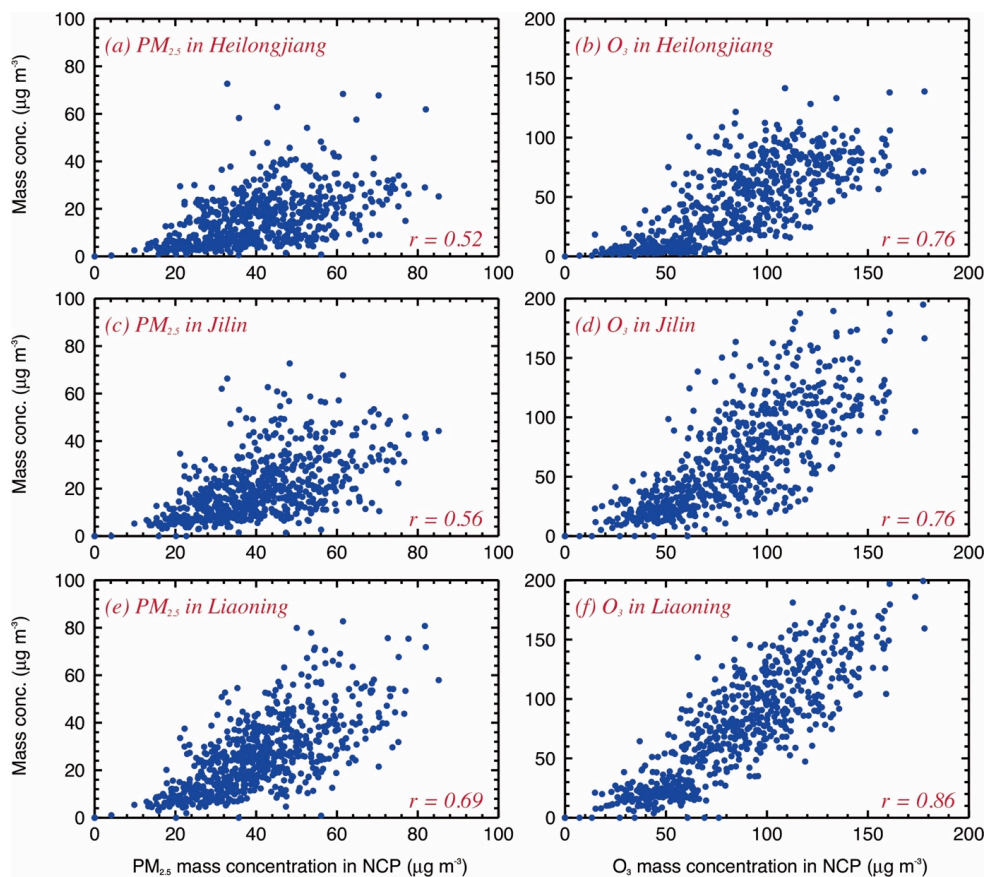
Atmospheric
Chemistry
and Physics
Discussions

639
640
Figure 3 Relationships of observed PM$_{2.5}$ and O$_3$ concentrations in NCP with those in the
NEC during May to September from 2013 to 2016.
643

644
645
646   Figure 4 Same as Figure 3, but for the NWC.
647
648
649
650
651

Atmospheric
Chemistry
and Physics
Discussions
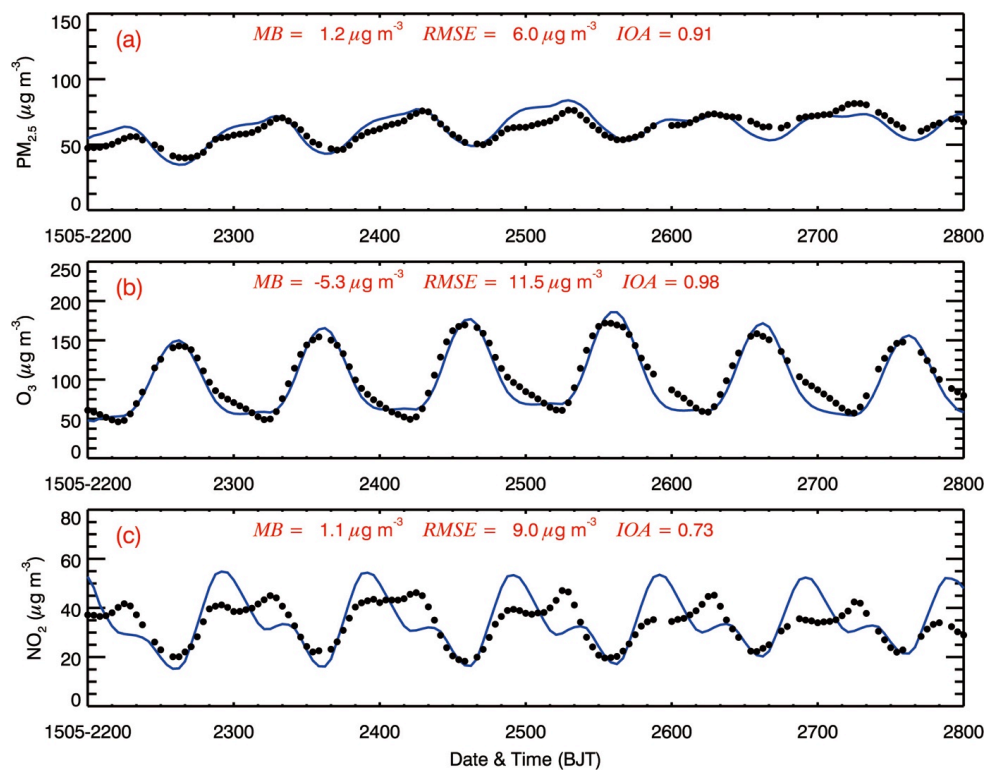
652
653
654 Figure 5 Comparison of measured (black dots) and predicted (blue line) diurnal profiles of
655 near-surface hourly (a) $PM_{2.5}$, (b) O_3, and (c) NO_2 averaged over all ambient monitoring
656 stations in Northern China from 22 to 28 May 2015
657
658
659
660
661
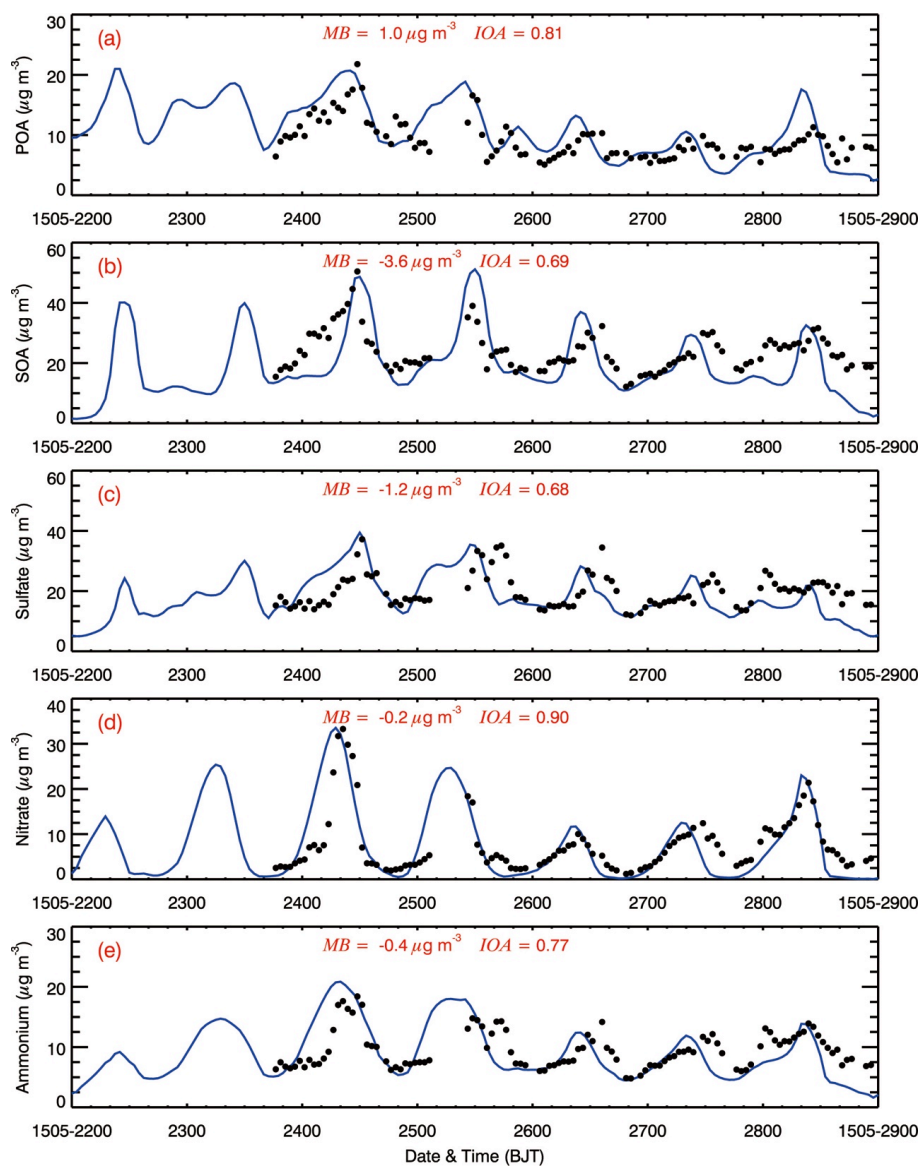
662

663

664 Figure 6 Comparison of measured (black dots) and simulated (black line) diurnal profiles of
665 submicron aerosol species of (a) POA, (b) SOA, (c) sulfate, (d) nitrate, and (e) ammonium at
666 NCNST site in Beijing from 22 to 28 May 2015.

667

668

669

670

671

Atmospheric
Chemistry
and Physics
Discussions

Open Access

672   o 10 sites   PM$_{2.5}$ concentration (μg m^{-3})   3.0 m s^{-1}
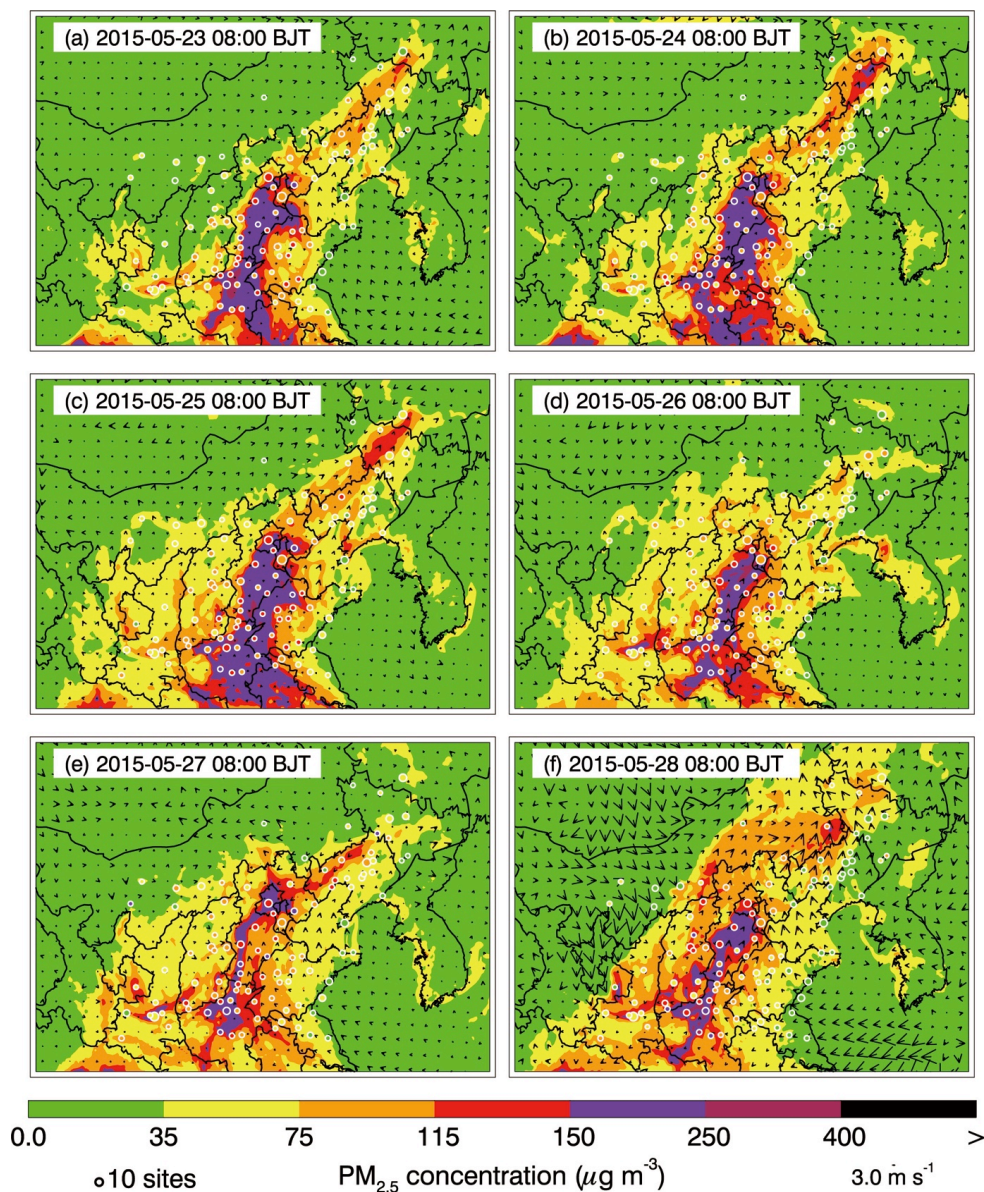
673 Figure 7 Pattern comparison of simulated vs. observed near-surface PM$_{2.5}$ at 08:00 BJT
674 during from 23 to 28 May 2015. Colored circles: PM$_{2.5}$ observations; color contour: PM$_{2.5}$
675 simulations; black arrows: simulated surface winds.
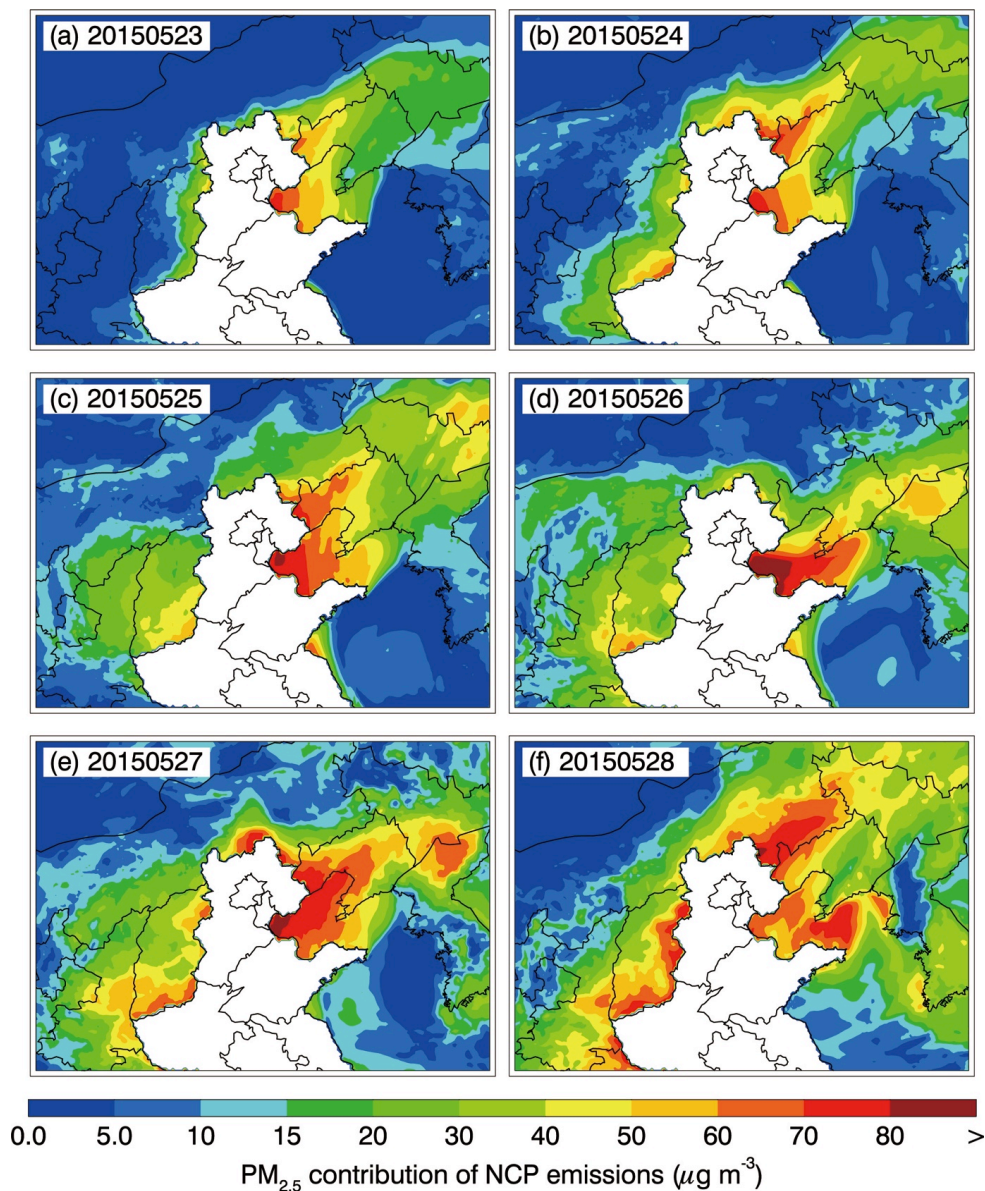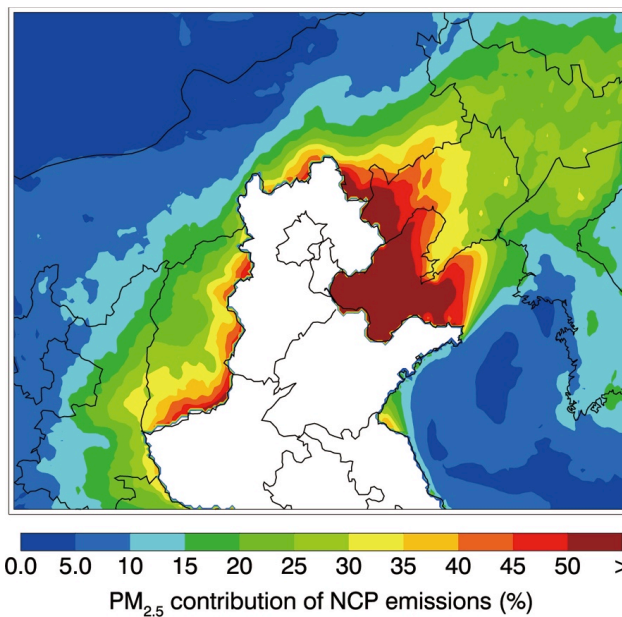676
677
678
679
680
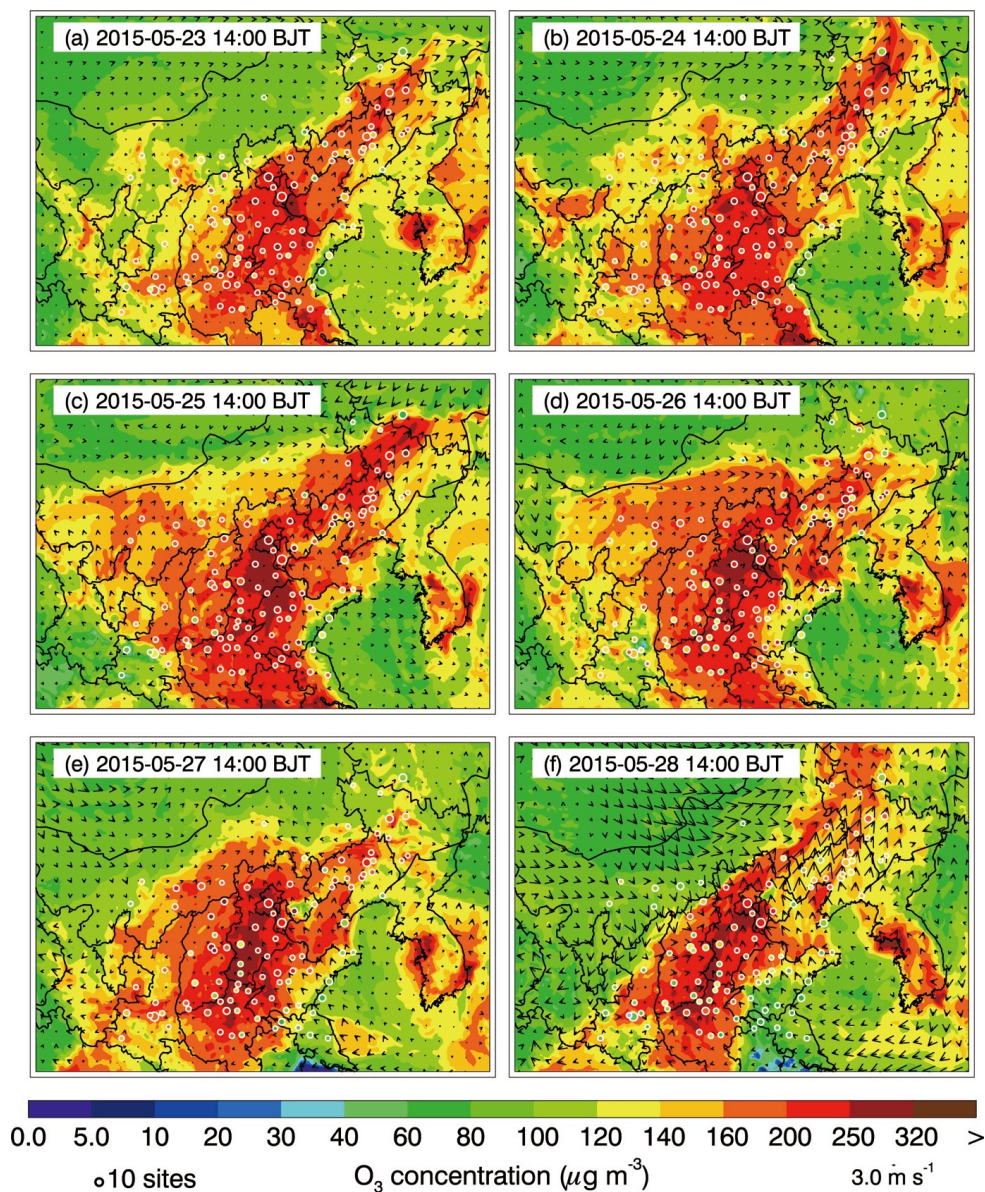
Figure 8 Same as Figure 7, but for the near-surface O$_3$ at 14:00 BJT.

Figure 9 Contributions of NCP emissions to the daily mean near-surface $PM_{2.5}$ concentration in the NEC and NWC from 23 to 28 May 2015.

Atmospheric
Chemistry
and Physics
Discussions

698
699 Figure 10 Average percentage contribution of NCP emissions to PM$_{2.5}$ concentrations in the
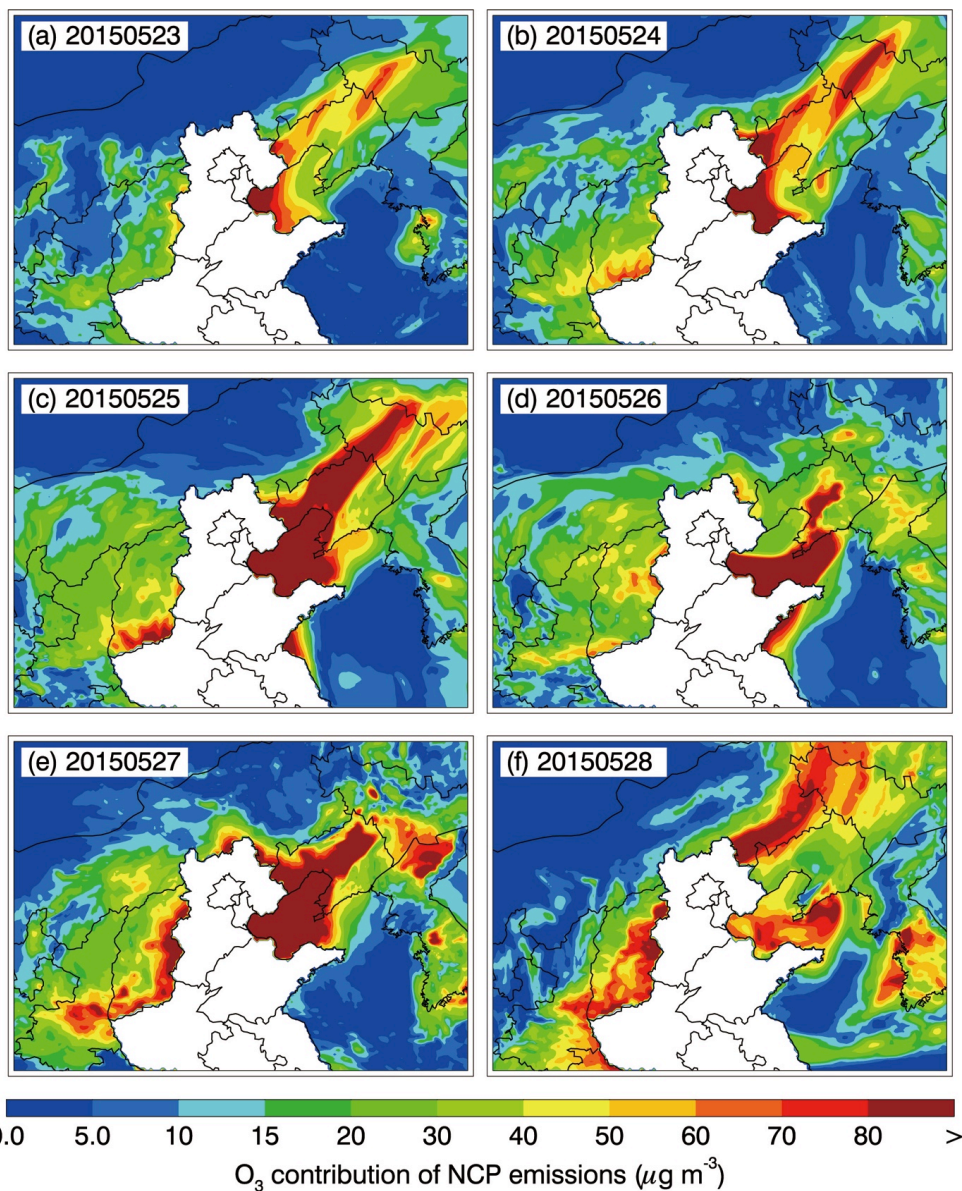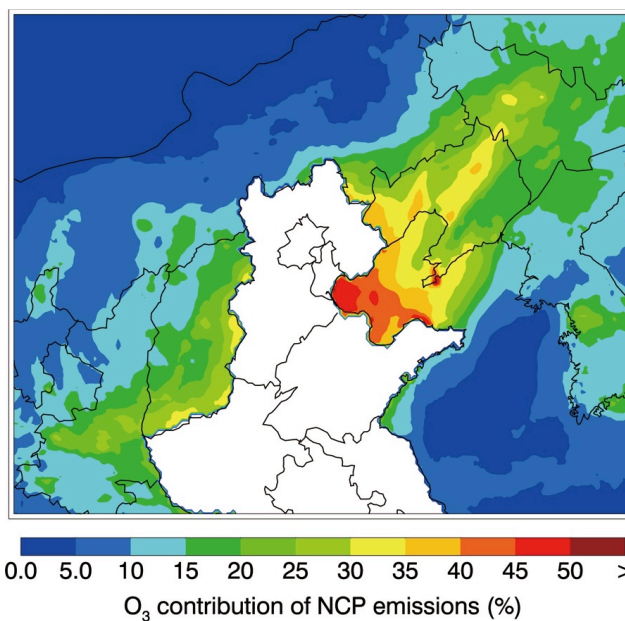700 NEC and NWC fron 22 to 28 May 2015.
701
702
703
704
705

Atmospheric
Chemistry
and Physics
Discussions

706
707
708 Figure 11 Same as Figure 9, but for the afternoon (12-18:00 BJT) O_3 concentration.
709
710
711
712
713

Atmospheric
Chemistry
and Physics
Discussions

714
715
716   Figure 12 Same as Figure 10, but for the afternoon (12-18:00 BJT) O_3 concentration.
717
718
719
720